

A Convection Chamber for Measuring Ice Crystal Growth Dynamics

Kenneth G. Libbrecht¹ and Helen C. Morrison

Department of Physics, California Institute of Technology
Pasadena, California 91125

Abstract. We present the design of a general-purpose convection chamber that produces a stable environment for studying the growth of ice crystals from water vapor in the presence of a background gas. Crystals grow in free fall inside the chamber, where the temperature and supersaturation are well characterized and surprisingly uniform. As crystals fall and land on a substrate, their dimensions are measured using direct imaging and broad-band interferometry. We also present a parameterized model of the supersaturation inside the chamber that is based on differential hygrometer measurements. Using this chamber, we are able to observe the growth and morphology of ice crystals over a broad range of conditions, as a function of temperature, supersaturation, gas constituents, gas pressure, growth time, and other parameters.

1 The Convection Chamber

The formation of complex structures during solidification often results from a subtle interplay of nonequilibrium, nonlinear processes, for which seemingly small changes in molecular dynamics at the nanoscale can produce large morphological changes at all scales. One popular example of this phenomenon is the formation of snow crystals, which are ice crystals that grow from water vapor in an inert background gas. Although this is a relatively simple physical system, snow crystals display a remarkable variety of columnar and plate-like forms, and much of the phenomenology of their growth remains poorly understood, even at a qualitative level [1].

To perform quantitative experimental investigations of ice crystal formation and morphological instabilities, one must create a stable growth environment, typically an inert background gas with a fixed temperature and humidity. For studying growth in near-atmospheric conditions, this requires temperatures of typically -40 C to 0 C, pressures of order 1 bar, and supersaturations of typically 0-20 percent. Since a nonzero supersaturation is an intrinsically nonequilibrium state, producing well-determined growth conditions with sufficient accuracy and stability is often a significant experimental challenge.

We have constructed a basic convection chamber for this purpose, shown schematically in Figure 1. The chamber consists of a stainless steel vacuum tank with an inside diameter of 53 cm and an inside height of 81 cm, and thus an interior volume of 179 liters. The outside of the chamber is covered (including the sides and both ends) by 3-mm thick copper plates with soldered cooling pipes. A programmable chiller cools the plates by circulating methanol through the soldered pipes. Once the system is stable, the chiller can maintain the interior temperature of the chamber down to -35 C with an accuracy of about 0.1 C.

An insulated water reservoir, also shown in Figure 1, is placed at the bottom of the tank to provide a source of water vapor. The water reservoir has an inside diameter of 14.5 cm and a depth of 5 cm, and it is typically filled with 0.8 liters of deionized water. The water temperature is servo controlled to an accuracy of approximately 0.25 C. The heated water drives convection inside the chamber that mixes water vapor into the surrounding gas. In steady state this simple configuration provides a stable environment in which the temperature and supersaturation are surprisingly uniform over much of the interior of the chamber.

A pulse of rapidly expanding gas is used to nucleate the growth of ice crystals at the top of the chamber [2]. The

¹ e-mail address: kgl@caltech.edu; see also
<http://www.its.caltech.edu/~atomic/publist/kglpub.htm>

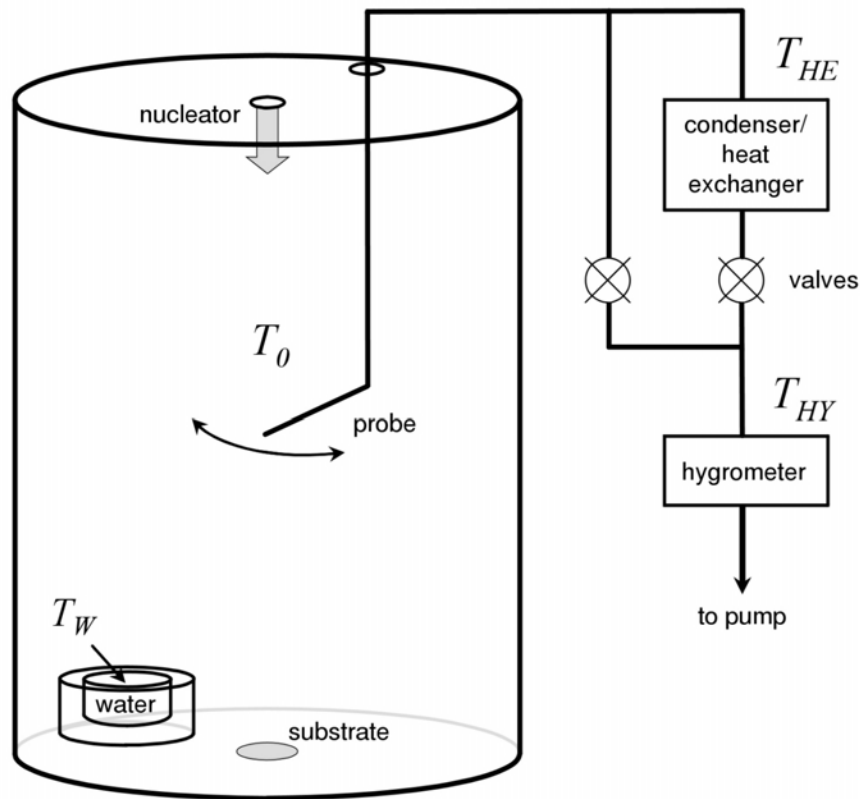


Figure 1. Schematic diagram of the growth chamber and differential hygrometer, as described in the text. The probe and water reservoir inside the chamber are drawn roughly to scale, whereas the hygrometer elements have been enlarged for clarity.

nucleator is made from a 5-cm-long pipe, 2 cm in diameter, with solenoid-actuated valves on both ends, connected to a source of compressed gas that has been saturated with water vapor. The pipe and valves are kept at approximately the same temperature as the chamber via simple conduction to the exterior cold plates. The first valve is opened to admit compressed gas into the pipe and then closed. The second valve is then opened to discharge the compressed gas into the growth chamber. The rapid expansion cools the saturated gas inside the pipe to nucleate small ice crystals [2]. We typically use nitrogen gas in the nucleator, although argon, helium, and other gases work as well. Typically about 10 psi is needed, with higher gas pressures producing more crystals.

The crystals grow in free fall in the supersaturated environment until a combination of gravity and convective currents causes some of them to fall onto a glass substrate at the bottom of the chamber. At this point the crystal dimensions can be measured from below using direct imaging and interferometry [3], described further below. This versatile chamber can produce a large number of crystals in a short time, allowing one to build up statistics on the growth and morphology as a function of temperature, supersaturation, gas constituents, gas pressure, growth time, and other parameters.

The temperature and supersaturation inside the chamber are measured using the probe and differential hygrometer set-up shown in Figure 1. The temperature probe is a calibrated thermistor with an absolute accuracy of 0.1C, located at the end of a sample tube placed halfway between the top and bottom of the chamber. Under typical conditions (chamber temperature T_0 between 0 C and -25 C with a pressure of one bar), we have found that the temperature is uniform to approximately 0.1 C as the probe is moved from side to side, even though on one side of the probe's travel it is directly over the water reservoir. The walls of the chamber are typically 2 C cooler than T_0 (since the warmer

water adds heat to the gas, which must be removed via contact with the walls), but this is only evident from the probe when it is within 2 cm of the walls. Convection efficiently mixes the gas inside the chamber to maintain this nearly uniform temperature.

Supersaturation is measured using a Vaisala HUMICAP hygrometer consisting of a thin-film polymer material that absorbs water vapor depending on the surrounding humidity, which is then determined by electronically measuring the dielectric properties of the film. The hygrometer sensor is placed inside a temperature-regulated enclosure kept at temperature T_{HY} (see Figure 1), and gas entering this enclosure has its temperature brought to T_{HY} before it contacts the hygrometer sensor.

A pump draws gas from the probe tube inside the chamber to the hygrometer at a rate of approximately $3 \text{ cm}^3/\text{sec}$, either directly or by first passing it through a condenser/heat-exchanger, as shown in Figure 1. (In operation, one valve is open while the other is closed.) The condenser/heat-exchanger consists of a thin copper tube soldered to a heat sink at temperature T_{HE} . The water content of gas that has passed through the condenser/heat-exchanger is equal to that of saturated gas at temperature T_{HE} . Care is taken that water does not condense anywhere inside the differential hygrometer except in the condenser/heat-exchanger. In particular, we heat the inside of the thin teflon probe tube inside the chamber using a coaxial heating wire, and we make sure all other flow tubes are at temperatures $T > T_0$.

We model the operation of this differential hygrometer by assuming the hygrometer measures

$$H = \frac{c_{input}}{c_{sat}(T_{HY})} + A$$

where c_{input} is the water content of the gas entering the hygrometer, $c_{sat}(T_{HY})$ is the water content of saturated gas at the hygrometer temperature T_{HY} , and A represents some nearly constant offset in the instrument. For a perfect hygrometer, we would have $A = 0$, so the formula then gives simply the relative humidity.

If we send gas from the probe directly into the hygrometer, we measure

$$H_1 = \frac{c_{probe}}{c_{sat}(T_{HY1})} + A$$

where c_{probe} is the water content of the gas entering the probe. If the gas first goes through the heat exchanger, then we measure

$$H_2 = \frac{c_{HE}}{c_{sat}(T_{HY2})} + A$$

where $c_{HE} = c_{sat}(T_{HE})$ is the water content after the gas has gone through the heat exchanger. Putting these together, we have

$$c_{probe} = [(H_1 - H_2) c_{sat}(T_{HY2}) + c_{sat}(T_{HE})] \frac{c_{sat}(T_{HY1})}{c_{sat}(T_{HY2})}$$

and this in turn gives the supersaturation inside the tank

$$\sigma = \frac{c_{probe} - c_{sat}(T_{probe})}{c_{sat}(T_{probe})}$$

By using a differential measurement, we eliminate A and thus increase the accuracy of our measurement.

In operation we first set $T_{HE} \approx T_0$ and set T_{HY} so that the water content of the gas in the chamber will produce a relative humidity (after being heated to T_{HY}) of approximately 50 percent. We then flow gas from the probe directly to the hygrometer and monitor H_1 , T_{HY1} , and T_0 until these quantities have stabilized (the hygrometer relaxation time is typically several minutes at temperatures near -15 C). Next we switch the valves and monitor H_2 , T_{HY2} , and T_{HE} until the readings are again stable, and then we repeat this sequence several times. A single hygrometer measurement sequence may take approximately one hour to complete, and our results are shown in Figure 2.

2 Modeling Supersaturation

We model the rate of evaporation of water into a closed chamber by [4, 5]

$$\frac{dc}{dt} \propto g(T_W, T_0)[c_{sat}(T_W) - c_{sat}(T_0)]$$

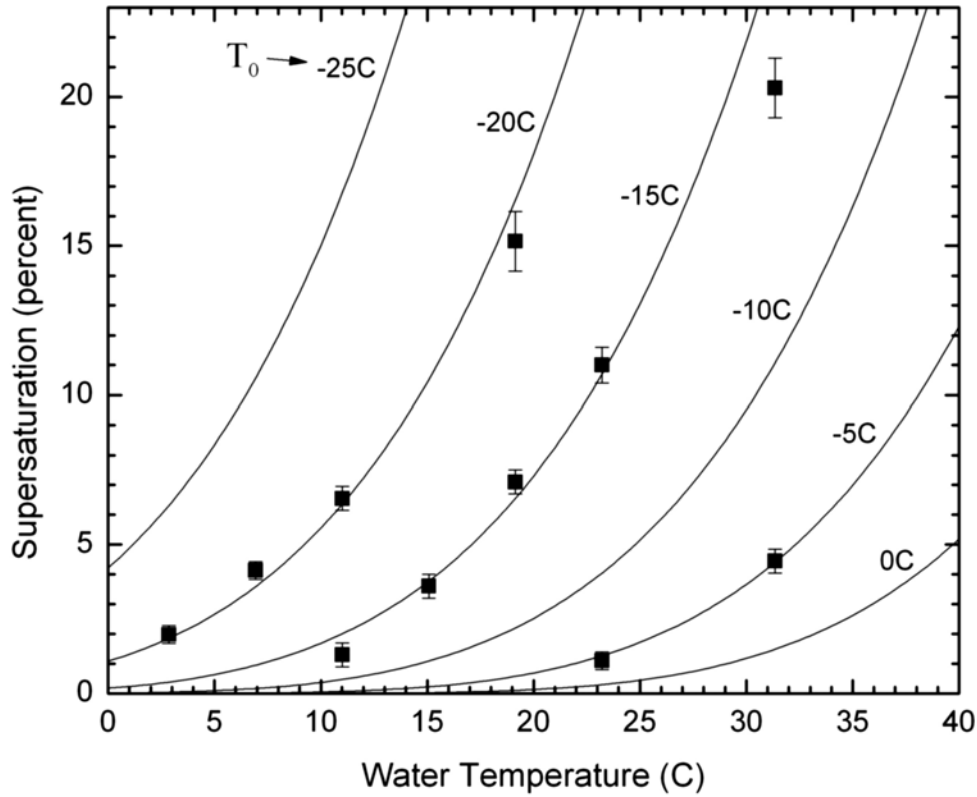


Figure 2. Supersaturation measurements taken in air at a pressure of one bar, at chamber temperatures of $T_0 = -5$ C, -15 C, and -20 C (points), along with model calculations at several temperatures (lines).

where the temperatures are defined above and in Figure 1. Here we include a dimensionless function $g(T_W, T_0)$ to describe the strength of convection inside the chamber. When $\Delta T = T_W - T_0$ is small, the resulting convection is weak, so little water vapor is carried into the chamber, whereas more vigorous convection will increase dc/dt . Thus we expect $g(T_W, T_0)$ will depend mainly on ΔT and will increase monotonically with ΔT .

In addition to evaporation, we also have condensation onto the walls, which we describe as

$$\frac{dc}{dt} \propto \sigma c_{sat}(T_0)$$

In steady-state, these two rates will be equal, giving

$$\sigma = g(T_W, T_0) \frac{c_{sat}(T_W) - c_{sat}(T_0)}{c_{sat}(T_0)}$$

To fit our measurements, we use

$$g(T_W, T_0) = 2.6(1 - e^{-\Delta T/30})^\alpha$$

with $\alpha = (0.11T_0 + 5.5)$, where ΔT and T_0 are measured in degrees Celsius. Although this functional form for $g(T_W, T_0)$ is *ad hoc* and includes several adjustable parameters, the resulting model fits our data well and provides physically reasonable trends with T_W and T_0 . We expect that the detailed form of $g(T_W, T_0)$ would likely change with a different chamber geometry or over a different temperature range. Using this model, we are able to interpolate between our hygrometer measurements to determine the supersaturation inside the growth chamber as a function of T_0 and T_W to an absolute accuracy of about 20 percent.

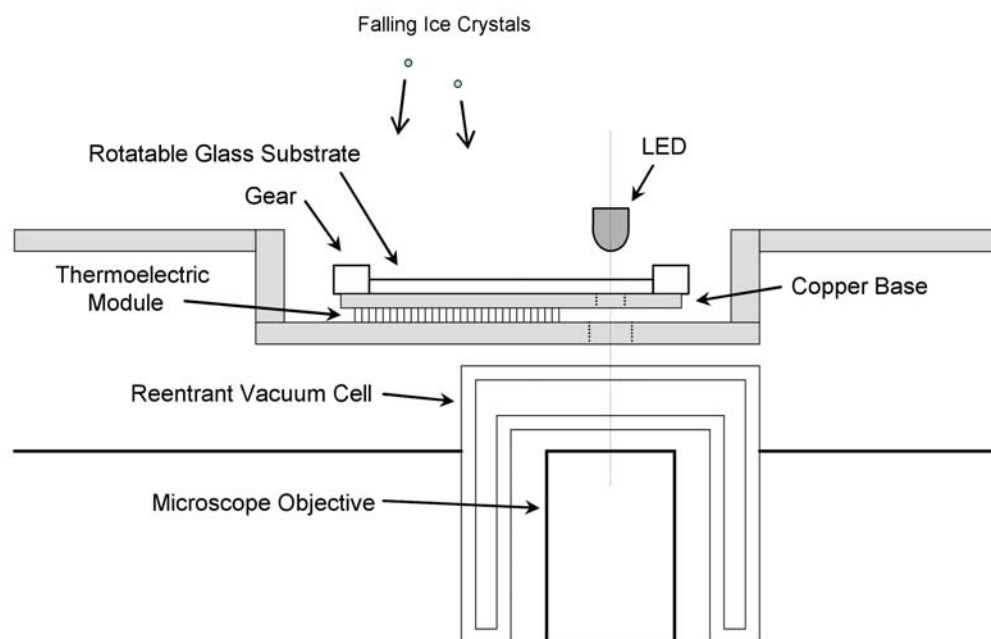


Figure 3. The substrate assembly at the bottom of the convection chamber. Ice crystals grow in free fall inside the chamber and some will fall onto the rotatable glass substrate where they can be measured.

3 Measuring Ice Crystals

After nucleation, ice crystals grow in free-fall inside the chamber until a combination of air currents and gravity carries some of them to a temperature-controlled glass substrate at the bottom of the chamber (see Figure 1). A schematic view of the substrate assembly is shown in Figure 3. The substrate itself is an uncoated glass window that has been glued to the center of a 5-cm-diameter Delrin spur gear. The substrate lies flat on a temperature-regulated copper base, and a drive gear (not shown in Figure 3) rotates the substrate about its vertical axis. An LED with a small diffusing screen provides illumination.

The rotating substrate solves a number of problems we had encountered earlier using a fixed substrate. First, the LED provides ample illumination from a large solid angle without impeding the fall of crystals to most of the substrate. Calculations show that heating from the LED is negligible. Second, the observable annulus on the substrate has a large area compared to the microscope's field of view, making it possible to find crystals to observe even when their surface density is low. This is important because nucleating a large number of crystals can significantly reduce the supersaturation inside the chamber, adding uncertainty to the growth measurements. Finally, this geometry makes it relatively easy to clean the substrate. This is accomplished by inserting a moistened Q-tip on a long rod from the top of the chamber. A mechanical guide (not shown in Figure 3) positions the Q-tip at one point on the observable annulus of the substrate. Once the Q-tip is resting on the glass, we rotate the substrate to drag-wipe the surface.

We use a Mitutoyo M Plan Apo 10X microscope objective, since this provides roughly $1\text{-}\mu\text{m}$ resolution with a 30-mm working distance. The objective is mounted on a 3-axis stage, and two video cameras provide low- and high-magnification views, the former with a field of view of approximately 3 mm. The low-magnification view is useful for finding crystals on the substrate, which are then observed more closely at high magnification. A reentrant evacuated cell with coated windows provides insulation between the microscope objective, which is at room temperature, and the cold substrate. A second copper base beneath the substrate base plate is separately cooled to ensure that the temperature of all parts surrounding the substrate remain uniform and stable during observations.

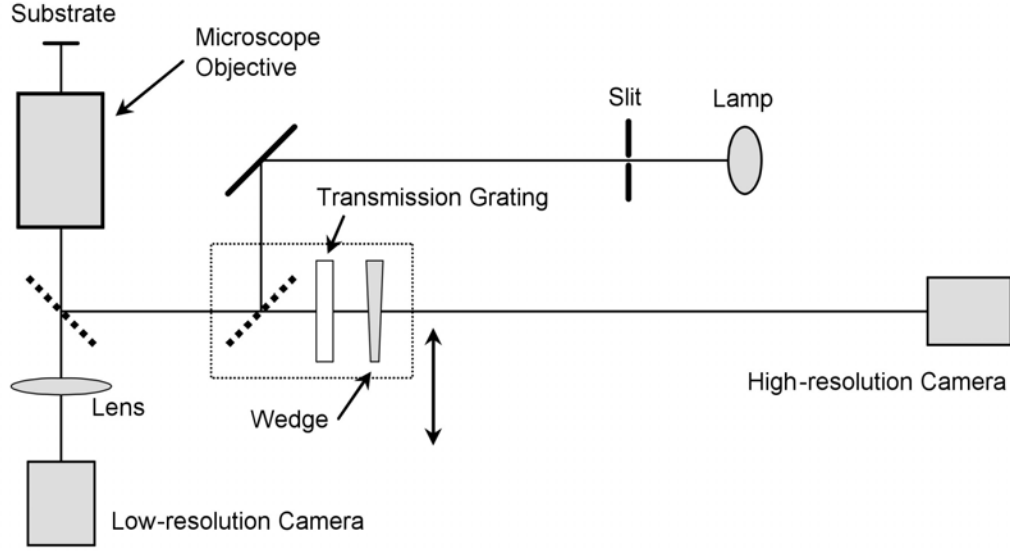


Figure 4. Optical layout for measuring the size and thickness of crystals landing on the substrate. For direct imaging at high and low resolution, the transmission grating assembly (shown in a box) is moved out of the optical path. When this assembly is in place (shown), the high-resolution camera records the broad-band interferometer spectrum described in the text.

Thin, plate-like ice crystals tend to land flat on the substrate, with their broad faces contacting the glass, so their thickness cannot be easily measured using microscopy from below. Furthermore, the plates often have thicknesses of 1-2 μm , which is too small to be accurately measured using direct imaging. For such crystals, we use broad-band optical interferometry to measure thickness, with the optical layout shown in Figure 4. Light from an incandescent bulb passes through a rectangular slit, and the slit is imaged by the microscope objective onto the ice crystal. Some of the incident light reflects off the glass-ice boundary, and more reflects off the ice-air boundary. Amplitudes of the two reflections add with an additional phase equal to $\varphi = 4\pi hn/\lambda$, where h is the ice thickness and $n(\lambda)$ is the index of refraction of ice at wavelength λ . The resulting reflected intensity is

$$\begin{aligned} I &\sim |R_1 + R_2 e^{i\varphi}|^2 \\ &\sim (1 + r^2) + 2r \cos \varphi \\ &\sim (1 + \cos \frac{4\pi hn}{\lambda}) \end{aligned}$$

where $r = R_2/R_1$ is the ratio of reflection amplitudes, which depends on the index jumps at the two interfaces. We have taken $r \approx 1$ for the last expression because the index of refraction of ice is approximately midway between those of air and glass. Note that the limit $h \rightarrow 0$ gives the maximum reflected intensity, because the air-glass interface has the largest index jump and thus produces the largest reflected intensity.

The reflected light is dispersed by a transmission grating (see Figure 4), and the interference spectrum is viewed by the high-resolution camera. Figure 5 shows a series of interference spectra taken as a plate-like crystal slowly evaporated away, along with a set of calculated spectra. Calibration for the calculations was obtained by shining red ($\lambda = 654 \text{ nm}$) and green ($\lambda = 532 \text{ nm}$) laser pointers through the slit and observing where the resulting spots appeared on the video image.

We use three techniques to infer crystal thickness from the interferometer spectra: 1) direct comparison of the video image with model spectra, as shown in Figure 5; 2) simply counting fringes on the video image; and 3) measuring the fringe spacing at the red end of the spectrum on the video image. When the crystal thickness is $h < 2$

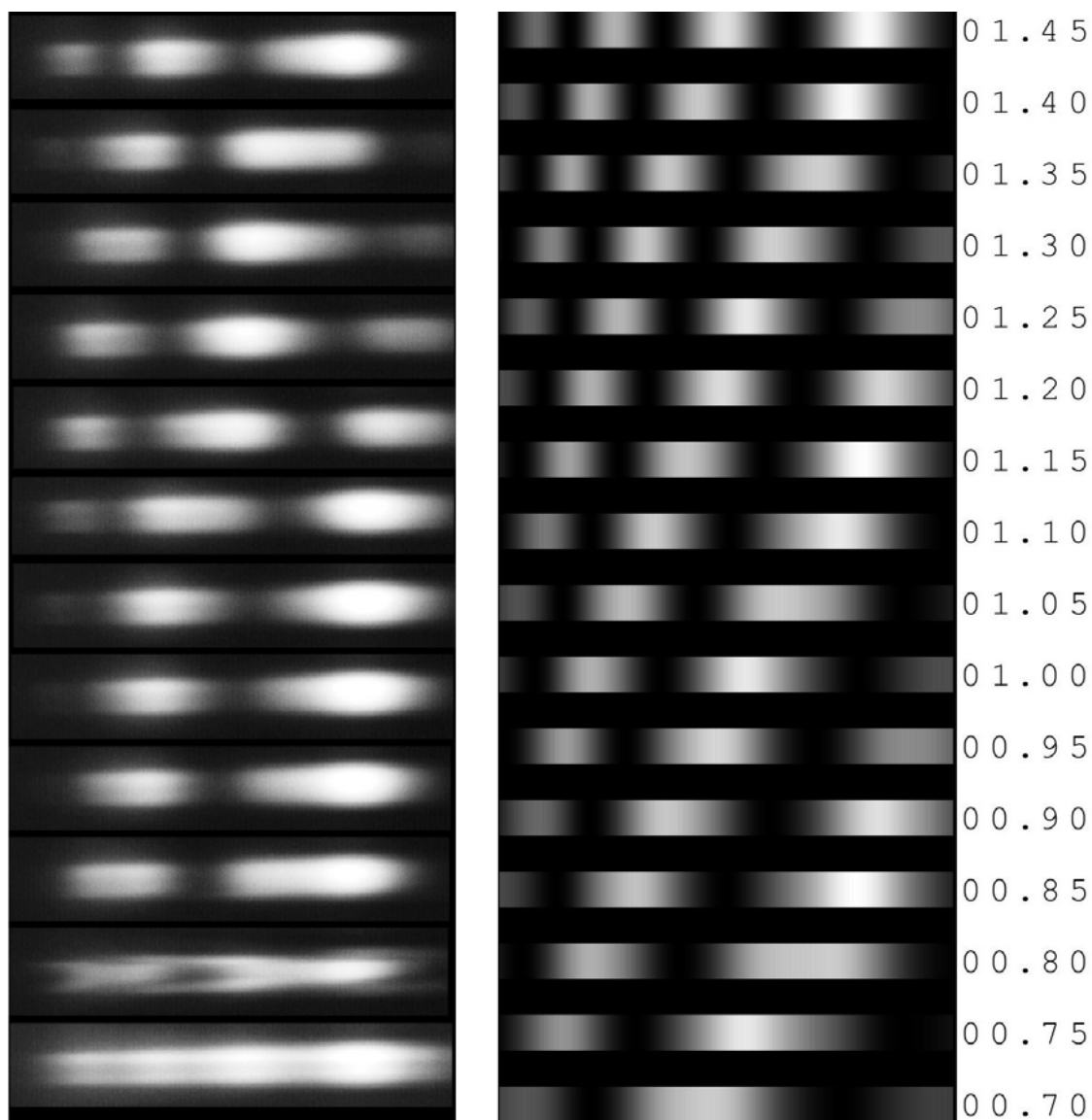


Figure 5. The left panel shows a series of interferometer spectra taken as a plate-like ice crystal slowly evaporated from the substrate. The right panel shows a series of calculated spectra, each labeled with the modeled ice thickness in microns. In both cases the spectra cover the range from 440 to 820 nm. Comparing the top spectrum on the left with the set of calculated spectra reveals that the crystal started with a thickness of approximately $1.1\ \mu\text{m}$. After some evaporation, the 10th spectrum shows the crystal with a thickness of $0.8\ \mu\text{m}$. After this, the lateral size of the crystal diminished to where it was smaller than the imaged slit, giving the next-to-last spectrum. The last spectrum was taken after the crystal had evaporated away completely. Here the residual brightness variations result from the lamp spectrum along with weak accidental etalons within the optics.

μm , direct comparison with model spectra is the only technique that yields accurate data, but this method is quite slow to use. When the thickness is $1 < h < 4 \mu\text{m}$, simply counting fringes on the video image yields data with roughly 10 percent accuracy, which is sufficient for our requirements. However, counting cannot be used for still thicker crystals because the fringes tend to merge together at the green end of the spectrum. Therefore, when $3 < h < 15 \mu\text{m}$, we measure the fringe spacing at the red end of the spectrum on the video image. With proper calibration of the three techniques, we are able to quickly and easily measure crystal thicknesses over the range $0.5 < h < 15 \mu\text{m}$ with overall absolute accuracies of 20 percent or better.

4 Operation

A typical run with this apparatus begins with sealing the chamber and cooling it to the set temperature, which takes several hours. The air may be pumped out and replaced with another gas as desired. When the temperature is stable, we add water to the reservoir and wait for it to reach its set temperature. In general, the temperature of the gas inside the chamber depends on both the temperature of the chamber walls (the chiller set point) and the water temperature.

Care must be taken to ensure that the chamber walls are covered fairly uniformly with ice, in order to produce well-defined boundary conditions for realizing a stable and known supersaturation. When operating the chamber above -15°C , we first cool the chamber to -15°C for several hours to make sure any water droplets condensed on the walls are frozen. Also, we repeatedly nucleate many crystals immediately after adding room-temperature water to the reservoir, so that some will attach to the chamber walls.

The number of crystals produced by a single cycle of the nucleator is a strong function of the nucleator gas pressure, with higher pressures producing more crystals. We typically run with 5-15 psi and adjust this so it is within 1-2 psi of the point when crystals first appear. By measuring the mass of a typical falling crystal and the number of crystals on the substrate after a single nucleation cycle, we estimate that the supersaturation is not substantially reduced by the growing crystals, provided we keep the nucleation pressure low.

Once an ice crystal lands on the substrate, it will grow or evaporate with time, depending on the substrate temperature. In practice, we have found that the substrate temperature must remain within a few hundredths of a degree of the zero-growth temperature to keep crystals from growing significantly after 1-2 minutes on the substrate. We minimize the adverse effects of growth or evaporation on the substrate by observing crystals as quickly as possible after they have fallen. After nucleating a set of crystals inside the chamber, we monitor the substrate while searching for fallen crystals, continually recording the video output to DVD. Each time a crystal is spotted on the low-res camera, it is moved to the high-res camera for measurement, and its thickness is recorded with the interferometer, which all takes just a few seconds. The growth time is assumed to be the elapsed time between nucleation and observation, ignoring the short residence time of crystals on the substrate. When crystals first begin to fall, we measure them all; after about a minute we record only the larger ones for a short additional time. This strategy usually allows us to record 1-2 dozen crystals in a single nucleation cycle. If observations of long growth times are desired, we use the same measurement strategy, except we use a shutter to keep crystals off the substrate for some period of time before beginning observations. Under typical conditions, all the crystals will fall after 5-10 minutes.

Our experience with this general-purpose convection chamber indicates that it can produce a stable environment in which the temperature and supersaturation are easily controlled and surprisingly uniform. Ice crystals grown in the chamber exhibit a good uniformity with respect to size and morphology. Measurement accuracies of 10-20% (in crystal size and thickness, as well as chamber supersaturation) are routinely achieved. Since the chamber is easy to use and can produce a wide variety of environmental conditions, we are finding it quite useful for investigating the detailed physics of ice crystal growth.

5 Acknowledgements

We acknowledge support for HCM by the Summer Undergraduate Research Fellowship (SURF) program and the CamSURF program at Caltech.

6 References

- [1] K. G. Libbrecht, "The physics of snow crystals," Rep. Prog. Phys. 68, 855-895 (2005).
- [2] T. C. Foster and J. Hallett, "Ice crystals produced by expansion: experiments and application to aircraft-produced ice," J. Appl. Meteor. 32, 716-728 (1993).
- [3] K. G. Libbrecht, "Precision measurements of ice crystal growth rates," arXiv:cond-mat/0608694v1 (2006).
- [4] J. P. Hirth and G. M. Pound, "Condensation and evaporation - nucleation and growth kinetics," (New York: Macmillan) (1963).
- [5] M. W. Zemansky and R. H. Dittman, "Heat and thermodynamics - an intermediate textbook," (New York: McGraw-Hill) (1997).